Composite Structures 200 (2018) 187–194

Contents lists available at ScienceDirect

Composite Structures

journal homepage: www.elsevier.com/locate/compstruct

Edge effects in adhesively bonded composite joints integrated with piezoelectric patches

S.A. Yousefsani, M. Tahani*

Department of Mechanical Engineering, Faculty of Engineering, Ferdowsi University of Mashhad, Mashhad, Iran

ARTICLE INFO

Keywords:
Adhesive joint
Laminated composite
Stress analysis
Edge effect
Full layerwise theory
Piezoelectric

ABSTRACT

Analytical electromechanical solutions to the interfacial stresses in the adhesively bonded composite joints integrated with piezoelectric actuator are presented in this paper within the framework of full layerwise theory. Two lap joints with and without interfacial void are studied, and the edge effects near the end-points of the bondline as well as around the void are investigated. Sets of fully coupled governing equations of equilibrium are derived using the principle of minimum total potential energy and are simultaneously solved using the state space approach. It was observed that the edge effects results in significant interfacial stress concentrations around the void edges that may cause propagation of microcracks and debonding.

1. Introduction

Linear piezoelectricity is a mutual interaction of electromechanical characteristics of non-centric crystals [1]. In piezoelectric materials, an external electric charge causes molecular polarization, and the consequent dielectric displacement results in deformation. This property facilitates the use of piezoelectric materials as actuators in applications like ultrasound acoustic wave generators, quartz clocks, and smart joints. Piezoelectric sensors and transducers are also integrated with the composite structures, such as adhesive joints in aircraft wings, for the structural health monitoring [2–7] as well as debonding and fatigue damage identification [8–12].

Nowadays, nondestructive health monitoring is vital for engineering structures, and hence there is an increasing demand on use of smart structures such as piezo-embedded systems. Piezoelectric patches are generally joined to the underlying composite substrates using adhesive bonding. During deformation of an adhesively bonded composite joint, the interfacial shearing and peeling stresses (as a result of difference in the stiffness of adherends) distribute on large surfaces decreasing the stress concentrations. However, at small regions around the end-points of bonded zone the edge effects result in locally high stress peaks [13–16]. This is also the case when there is an interfacial void within the bonding zone [17,18]. A void (also referred to as a gap) is a region in the bonding layer where no adhesive exists between the substrates as a result of adhesive evaporation or inappropriate manufacturing process [17].

The quality of adhesive bonding between the substrate and relying piezoelectric patch is of a substantial importance in adhesively bonded joints, since the failure of bonding results in malfunction of the smart structure. In stress analysis of adhesive joints, therefore, it is inevitable to accurately determine how the edge effects can increase the localized interfacial stress concentrations which may cause debonding and joint failure. Although no experimental method is available to determine the interfacial stresses, there is a number of analytical/numerical studies on the interlaminar stress analysis of piezoelectric bonded sandwich panels, laminated beams and plates, piezoelectric bimorphs, and adhesive joints integrated with piezoelectric patches [19–24].

Kapuria [25] presented a coupled electromechanical analysis of laminated composite beams with piezoelectric layers in which the displacement components and the electric charge are approximated by the third-order zigzag theory and layerwise interpolation function, respectively. In this study, the equations of static equilibrium are derived by the principle of virtual work and solved using the Fourier series. Based on the Euler-Bernoulli beam theory, Luo and Tong [26,27] presented analytical solutions for static loading of a beam (fully or partially) integrated with a piezoelectric patch. They solved the governing ordinary differential equations assuming the solutions as exponential functions.

Cheng and Taheri [28] investigated the stress field in bonding region of a smart adhesively bonded piezoelectric joint using the first-order shear deformation theory, and studied the effects of position and size of piezoelectric patches. Cheng et al. [29] developed a smart adhesively bonded single-strap joint integrated with piezoelectric patches (as actuator and sensor) in order to reduce the interfacial peel and shear stresses within the bonding layer. In this study, the coupled second-order differential equations governing the static equilibrium were

* Corresponding author at: Department of Mechanical Engineering, Ferdowsi University of Mashhad, P.O. Box: 91775-1111, Mashhad, Iran.
E-mail address: mtahani@um.ac.ir (M. Tahani).

https://doi.org/10.1016/j.compstruct.2018.05.071
Received 19 October 2017; Received in revised form 23 January 2018; Accepted 17 May 2018
Available online 18 May 2018

derived based on the first-order shear deformation theory and solved using the state-space approach. They also presented analytical solutions for tubular composite joints integrated with piezoelectric patches under different loading scenarios (i.e., tension, bending and torsion) based on the Levy solutions [30–32].

Jin and Wang [33] presented two-dimensional analysis of a piezoelectric patch bonded to a semi-infinite substrate assuming constant shear stress through the thickness of adhesive layer. This is also the case for the analytical model presented by Liang et al. [34] where they modeled the composite beam and the piezoelectric layer with the Timoshenko beam theory and considered the adhesive layer as a continuous spring with normal and shear stiffness. But it was previously shown that the shear and peel stresses exhibit nonlinear variations through the adhesive thickness particularly near the edges [15]. This is more evident in thick laminated composite joints with significant variation of stiffness between layups and layers [14].

To meet the requirements of static equilibrium, the interlaminar stresses must continuously distribute through the joint thickness. However, simple analytical methods, like the equivalent single layer (ESL) theories, assume the displacement fields as a continuous function of thickness coordinate resulting in discontinuous interlaminar stresses between different layups/layers. Therefore, they cannot capture the real through-thickness stress variations. Instead, the full layerwise theory (FLWT), as an advanced theory of three-dimensional elasticity, can capture the actual nonlinear variations of interfacial stresses through the thickness giving more accurate predictions of stress distributions. In FLWT, the displacement field is of C^0-order of continuity (i.e., a continuous displacement field with discontinuous derivatives with respect to thickness coordinate) resulting in continuous stresses at the interfaces of dissimilar layups/layers through the joint thickness.

This paper presents an analytical electromechanical study on the edge effects and interfacial stress distributions in adhesively bonded composite joints integrated with piezoelectric actuator within the framework of full layerwise theory. Two benchmarks including simple lap joints with and without an interfacial void are modeled, and the edge effects near the end-points of the bondline as well as around the void are investigated. To assign the layerwise displacement field, each joint is divided into a number of mathematical (virtual) plies through its thickness. By dividing the geometry of proposed joints into distinct regions along its length, including the in-bonding and out-of-bonding regions, sets of coupled equations of equilibrium and the associated boundary and continuity conditions are derived using the principle of minimum total potential energy. Upon appropriate definition of stress resultants, governing equations of equilibrium then are obtained for each region in terms of layerwise displacement field. Finally, sets of fully coupled governing equations of equilibrium are assembled together in the matrix form and simultaneously solved using the state space approach.

2. Method

Fig. 1 illustrates a schematic view of a typical piezoelectric bonded joint with free-free boundary conditions. The sample joints without and with an interfacial void are denoted by J-1 and J-2 configurations corresponding to $L_V = 0$ and $L_V \neq 0$, respectively. Without loss of generality, it is assumed that both joints are symmetric with respect to z-axis, and hence, for sake of simplicity, they are modeled in half (i.e., for $x \geq 0$), and symmetrical boundary conditions are imposed to the right end at $x = 0$.

The joint length along x-axis is divided into two and three regions for J-1 and J-2 configurations, respectively. The sets of equations of equilibrium and the associated boundary/continuity conditions are presented here for one region only (e.g., region I in Fig. 1: $0 \leq x \leq L_V$), and all other regions have similar equations.

2.1. Layerwise displacement field

To assign the layerwise displacement field, first of all the joint thickness $H = t_P + t_A + t_S$ should be virtually divided into N mathematical plies with equal thickness of $h = H/N$. The number of mathematical plies is not limited to a specific value; however, it will be shown that there is no need to consider a large number of mathematical plies.

Considering that the joint width (in y-direction) is small, the layerwise displacement field is assumed as functions of only x- and z-coordinates as:

$$(u_1(x,y,z),u_2(x,y,z),u_3(x,y,z)) = (U_k(x),V_k(x),W_k(x))\Phi_k(z), \quad k = 1,2,...,N+1 \tag{1}$$

where summation convention are imposed on repetitive indices (or dummies) from 1 to $N + 1$, u_i ($i = 1, 2, 3$) represent the displacement components of an arbitrary point in undeformed configuration in the x-, y-, and z-coordinates, respectively, U_k, V_k, and W_k stand for the displacement components of any point on the kth virtual surface, and $\Phi_k(z)$ is a continuous interpolation function of z-coordinate through the thickness. The linear interpolation function with C^0 order of continuity at the interface of two adjacent virtual plies (as shown in Fig. 2) is used here. That is,

$$\Phi_k(z) = \begin{cases} 0 & z \leqslant z_{k-1} \\ \phi^2_{k-1}(z) & z_{k-1} \leqslant z \leqslant z_k \\ \phi^1_k(z) & z_k \leqslant z \leqslant z_{k+1} \\ 0 & z \geqslant z_{k+1} \end{cases}, \quad k = 1,2,...,N+1 \tag{2}$$

in which the local Lagrangian interpolation functions, ϕ^j_k ($j = 1,2$), are defined as:

$$(\phi^1_k,\phi^2_k) = ((z_{k+1}-z),(z-z_k))/h \tag{3}$$

Substitution of the layerwise displacement components into the linear strain-displacement relationships gives:

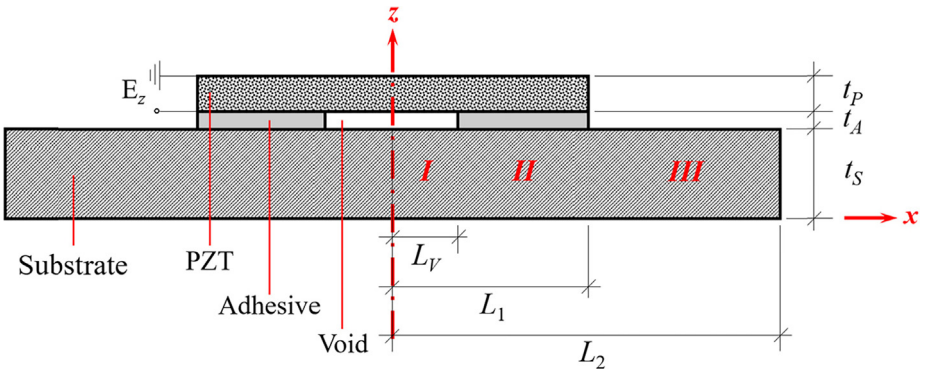

Fig. 1. Free-ends adhesively bonded joint integrated with piezoelectric actuator with and without interfacial void.

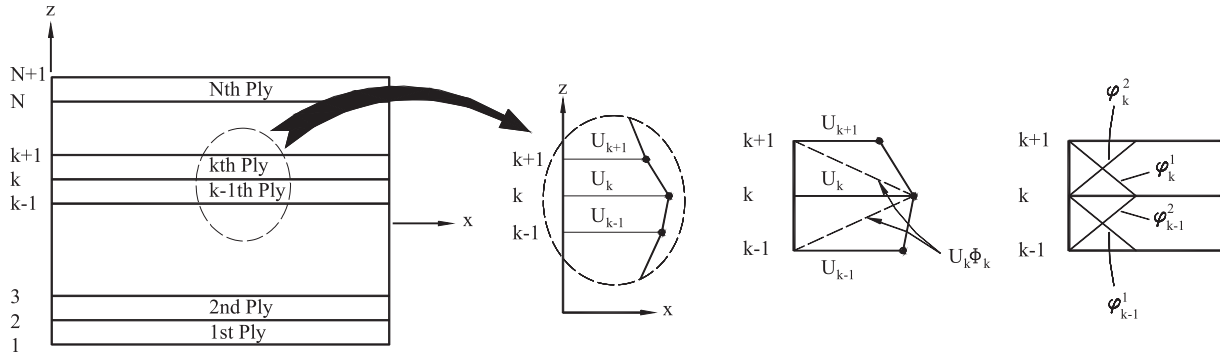

Fig. 2. Schematics of the joint thickness divided into N mathematical plies and the graphical representation of layerwise displacement field with C^0 order of continuity at the interface of adjacent plies based on definition of linear Lagrangian interpolation functions ϕ^1_k and ϕ^2_k.

$$\begin{cases} \varepsilon_x = \Phi_k \mathrm{d}U_k/\mathrm{d}x \\ \varepsilon_y = 0 \\ \varepsilon_z = W_k \mathrm{d}\Phi_k/\mathrm{d}z \end{cases}, \quad \begin{cases} \gamma_{yz} = V_k \mathrm{d}\Phi_k/\mathrm{d}z \\ \gamma_{xz} = U_k \mathrm{d}\Phi_k/\mathrm{d}z + \Phi_k \mathrm{d}W_k/\mathrm{d}x \\ \gamma_{xy} = \Phi_k \mathrm{d}V_k/\mathrm{d}x \end{cases} \tag{4}$$

2.2. Equations of equilibrium

The equations of equilibrium for each region shown in Fig. 1 and the associated boundary conditions are obtained using the principle of minimum total potential energy. According to definition of layerwise stress resultants as:

$$\{(M^k_x, M^k_{xy}, R^k_x), (N^k_z, Q^k_x, Q^k_y)\} = \int \{(\sigma_x, \sigma_{xy}, \sigma_{xz})\Phi_k, (\sigma_z, \sigma_{xz}, \sigma_{yz})(\mathrm{d}\Phi_k/\mathrm{d}z)\}\mathrm{d}z \tag{5}$$

the equilibrium equations for each region are derived (details available in [14]) as:

$$\delta U_k: \mathrm{d}M^k_x/\mathrm{d}x - Q^k_x = 0 \quad \delta V_k: \mathrm{d}M^k_{xy}/\mathrm{d}x - Q^k_y = 0 \quad \delta W_k: \mathrm{d}R^k_x/\mathrm{d}x - N^k_z = 0 \tag{6}$$

and the conditions of symmetry (at $x = 0$), free-end boundary conditions, and the displacement and stress continuity conditions between adjacent regions (e.g., regions I and II) are obtained respectively as:

$$\begin{cases} \text{Symmetry:} & U_k = V_k = R^k_x = 0 \\ \text{Free-ends:} & M^k_x = M^k_{xy} = R^k_x = 0 \\ \text{Continuity:} & (U_k, V_k, W_k, M^k_x, M^k_{xy}, R^k_x)^I = (U_k, V_k, W_k, M^k_x, M^k_{xy}, R^k_x)^{II} \end{cases} \tag{7}$$

2.3. Material constitutive equations

Generally, for an orthotropic piezoelectric laminae as the kth virtual ply in the joint configuration the stress-strain relationship in linear elasticity is written as [35]:

$$\begin{Bmatrix} \sigma_x \\ \sigma_y \\ \sigma_z \\ \sigma_{yz} \\ \sigma_{xz} \\ \sigma_{xy} \end{Bmatrix}^{(k)} = \begin{bmatrix} \overline{C}_{11} & \overline{C}_{12} & \overline{C}_{13} & 0 & 0 & \overline{C}_{16} \\ \overline{C}_{12} & \overline{C}_{22} & \overline{C}_{23} & 0 & 0 & \overline{C}_{26} \\ \overline{C}_{13} & \overline{C}_{23} & \overline{C}_{33} & 0 & 0 & \overline{C}_{36} \\ 0 & 0 & 0 & \overline{C}_{44} & \overline{C}_{45} & 0 \\ 0 & 0 & 0 & \overline{C}_{45} & \overline{C}_{55} & 0 \\ \overline{C}_{16} & \overline{C}_{26} & \overline{C}_{36} & 0 & 0 & \overline{C}_{66} \end{bmatrix}^{(k)} \begin{Bmatrix} \varepsilon_x \\ \varepsilon_y \\ \varepsilon_z \\ \gamma_{yz} \\ \gamma_{xz} \\ \gamma_{xy} \end{Bmatrix}^{(k)} - \begin{bmatrix} 0 & 0 & \overline{e}_{31} \\ 0 & 0 & \overline{e}_{32} \\ 0 & 0 & \overline{e}_{33} \\ \overline{e}_{14} & \overline{e}_{24} & 0 \\ \overline{e}_{15} & \overline{e}_{25} & 0 \\ 0 & 0 & \overline{e}_{36} \end{bmatrix}^{(k)} \begin{Bmatrix} \mathrm{E}_x \\ \mathrm{E}_y \\ \mathrm{E}_z \end{Bmatrix}^{(k)} \tag{8}$$

where $[\overline{C}]^{(k)}$ and $[\overline{e}]^{(k)}$ are the matrices of elastic stiffness and piezoelectric coupling of the kth ply in the rotated coordinate system and $\{\mathrm{E}\}^{(k)}$ is the vector of external electric field. Assuming that the electric field vector has a non-zero component in the z-direction only (i.e., $\mathrm{E}_x = \mathrm{E}_y = 0$), Eq. (8) can be rewritten in terms of strain components as:

$$[\overline{S}]^{(k)}\{\sigma\}^{(k)} = [\varepsilon_x - \overline{d}_{31}\mathrm{E}_z, \varepsilon_y - \overline{d}_{32}\mathrm{E}_z, \varepsilon_z - \overline{d}_{33}\mathrm{E}_z, \gamma_{yz}, \gamma_{xz}, \gamma_{xy} - \overline{d}_{36}\mathrm{E}_z]^{(k)^T} \tag{9}$$

in which we have $[\overline{S}]^{(k)} = [\overline{C}]^{(k)^{-1}}$ and $[\overline{d}]^{(k)} = [\overline{S}]^{(k)}[\overline{e}]^{(k)}$. Recalling Eq. (4), the strain in the y-direction, ε_y, is zero, and therefore, according to small width of joint and free lateral faces in the y-direction, it is safe to assume that σ_y equals zero through the joint width [36]. With this in mind, Eq. (8) can be rewritten as:

$$\begin{bmatrix} \overline{S}_{11} & \overline{S}_{13} & \overline{S}_{16} \\ \overline{S}_{13} & \overline{S}_{33} & \overline{S}_{36} \\ \overline{S}_{16} & \overline{S}_{36} & \overline{S}_{66} \end{bmatrix}^{(k)} \begin{Bmatrix} \sigma_x \\ \sigma_z \\ \sigma_{xy} \end{Bmatrix}^{(k)} = \begin{Bmatrix} \varepsilon_x - \overline{d}_{31}\mathrm{E}_z \\ \varepsilon_z - \overline{d}_{33}\mathrm{E}_z \\ \gamma_{xy} - \overline{d}_{36}\mathrm{E}_z \end{Bmatrix}^{(k)} \tag{10a}$$

$$\begin{bmatrix} \overline{S}_{44} & \overline{S}_{45} \\ \overline{S}_{45} & \overline{S}_{55} \end{bmatrix}^{(k)} \begin{Bmatrix} \sigma_{yz} \\ \sigma_{xz} \end{Bmatrix}^{(k)} = \begin{Bmatrix} \gamma_{yz} \\ \gamma_{xz} \end{Bmatrix}^{(k)} \tag{10b}$$

Inverting Eqs. (10) gives:

$$\begin{Bmatrix} \sigma_x \\ \sigma_z \\ \sigma_{xy} \end{Bmatrix}^{(k)} = \begin{bmatrix} \overline{\overline{C}}_{11} & \overline{\overline{C}}_{13} & \overline{\overline{C}}_{16} \\ \overline{\overline{C}}_{13} & \overline{\overline{C}}_{33} & \overline{\overline{C}}_{36} \\ \overline{\overline{C}}_{16} & \overline{\overline{C}}_{36} & \overline{\overline{C}}_{66} \end{bmatrix}^{(k)} \begin{Bmatrix} \varepsilon_x - \overline{d}_{31}\mathrm{E}_z \\ \varepsilon_z - \overline{d}_{33}\mathrm{E}_z \\ \gamma_{xy} - \overline{d}_{36}\mathrm{E}_z \end{Bmatrix}^{(k)} \tag{11a}$$

$$\begin{Bmatrix} \sigma_{yz} \\ \sigma_{xz} \end{Bmatrix}^{(k)} = \begin{bmatrix} \overline{\overline{C}}_{44} & \overline{\overline{C}}_{45} \\ \overline{\overline{C}}_{45} & \overline{\overline{C}}_{55} \end{bmatrix}^{(k)} \begin{Bmatrix} \gamma_{yz} \\ \gamma_{xz} \end{Bmatrix}^{(k)} \tag{11b}$$

where $\overline{\overline{C}}^{(k)}_{ij}$ $(i,j = 4,5)$ are the stiffness coefficients in the rotated coordinate system, and $\overline{\overline{C}}^{(k)}_{ij}$ $(i,j = 1,3,6)$ are defined as:

$$\begin{bmatrix} \overline{\overline{C}}_{11} & \overline{\overline{C}}_{13} & \overline{\overline{C}}_{16} \\ \overline{\overline{C}}_{13} & \overline{\overline{C}}_{33} & \overline{\overline{C}}_{36} \\ \overline{\overline{C}}_{16} & \overline{\overline{C}}_{36} & \overline{\overline{C}}_{66} \end{bmatrix} = \begin{bmatrix} \overline{S}_{11} & \overline{S}_{13} & \overline{S}_{16} \\ \overline{S}_{13} & \overline{S}_{33} & \overline{S}_{36} \\ \overline{S}_{16} & \overline{S}_{36} & \overline{S}_{66} \end{bmatrix}^{-1} \tag{12}$$

2.4. Governing equations of equilibrium

Rewriting the equations of equilibrium, Eq. (6), in terms of the displacement components results in the governing equations of equilibrium. To do so, first of all the strain components, Eq. (4), are substituted into Eq. (11), and then the results are substituted into Eq. (5) to write the stress resultants in terms of displacement components. That is,

$$(Q^k_y, Q^k_x, R^k_x) = (A^{kj}_{45}, A^{kj}_{55}, B^{kj}_{45})U_j + (A^{kj}_{44}, A^{kj}_{45}, B^{kj}_{55})V_j + (B^{jk}_{45}, B^{jk}_{55}, D^{kj}_{55})W'_j \tag{13a}$$

$$\left(\left(N^k_z + N^{k^E}_z\right), \left(M^k_x + M^{k^E}_x\right), \left(M^k_{xy} + M^{k^E}_{xy}\right)\right) = (\overline{B}^{jk}_{13}, \overline{D}^{kj}_{11}, \overline{D}^{kj}_{16})U'_j + (\overline{B}^{jk}_{36}, \overline{D}^{kj}_{16}, \overline{D}^{kj}_{66})V'_j + (\overline{A}^{jk}_{33}, \overline{B}^{kj}_{13}, \overline{B}^{kj}_{36})W_j \tag{13b}$$

Table 1
Mechanical and electrical properties of joint components.

	Composite	Adhesive		Piezoelectric
	Graphite-Epoxy	AY103		PZT-4
Elastic modulus (GPa)	$E_1 = 137.9$ $E_2 = E_3 = 14.48$	$E = 2.8$	Elastic stiffness (GPa)	$C_{11} = C_{22} = 139$ $C_{33} = 115$
Shear modulus (GPa)	$G_{12} = G_{13} = G_{23} = 5.86$	$G = E/2(1+\nu)$		$C_{13} = C_{23} = 74.3$ $C_{12} = 77.8$ $C_{44} = C_{55} = 25.6$ $C_{66} = 30.6$
Poisson's ratio (–)	$\nu_{12} = \nu_{13} = \nu_{23} = 0.21$	$\nu = 0.4$	Piezoelectric Constants ($C.m^{-2}$)	$e_{31} = e_{32} = -5.2$ $e_{33} = 15.1$

in which the equivalent stiffness matrices $\mathbf{A}^{kj}$, $\mathbf{B}^{kj}$, $\mathbf{D}^{kj}$, $\overline{\mathbf{A}}^{kj}$, $\overline{\mathbf{B}}^{kj}$, and $\overline{\mathbf{D}}^{kj}$ are defined as:

$$\begin{cases} A_{pq}^{kj} = \sum_{i=1}^{N} \int_{z_i}^{z_{i+1}} \overline{C}_{pq}^{(i)} \Phi'_k \Phi'_j \, dz \\ B_{pq}^{kj} = \sum_{i=1}^{N} \int_{z_i}^{z_{i+1}} \overline{C}_{pq}^{(i)} \Phi_k \Phi'_j \, dz \ , \quad pq = 4,5 \\ D_{pq}^{kj} = \sum_{i=1}^{N} \int_{z_i}^{z_{i+1}} \overline{C}_{pq}^{(i)} \Phi_k \Phi_j dz \end{cases} \tag{14a}$$

$$\begin{cases} \overline{A}_{pq}^{kj} = \sum_{i=1}^{N} \int_{z_i}^{z_{i+1}} \overline{\overline{C}}_{pq}^{(i)} \Phi'_k \Phi'_j \, dz \\ \overline{B}_{pq}^{kj} = \sum_{i=1}^{N} \int_{z_i}^{z_{i+1}} \overline{\overline{C}}_{pq}^{(i)} \Phi_k \Phi'_j \, dz \ , \quad pq = 1,3,6 \\ \overline{D}_{pq}^{kj} = \sum_{i=1}^{N} \int_{z_i}^{z_{i+1}} \overline{\overline{C}}_{pq}^{(i)} \Phi_k \Phi_j dz \end{cases} \tag{14b}$$

and the electrical stress resultants, $N_z^{k^E}$,$M_x^{k^E}$, and $M_{xy}^{k^E}$, are written as:

$$\begin{cases} N_z^{k^E} = \sum_{k=1}^{N} \int_{z_k}^{z_{k+1}} (\overline{\overline{C}}_{13}\overline{d}_{31} + \overline{\overline{C}}_{33}\overline{d}_{33} + \overline{\overline{C}}_{36}\overline{d}_{36})^{(k)} \mathrm{E}_z^{(k)} (d\Phi_k/dz) dz \\ M_x^{k^E} = \sum_{k=1}^{N} \int_{z_k}^{z_{k+1}} (\overline{\overline{C}}_{11}\overline{d}_{31} + \overline{\overline{C}}_{13}\overline{d}_{33} + \overline{\overline{C}}_{16}\overline{d}_{36})^{(k)} \mathrm{E}_z^{(k)} \Phi_k dz \\ M_{xy}^{k^E} = \sum_{k=1}^{N} \int_{z_k}^{z_{k+1}} (\overline{\overline{C}}_{16}\overline{d}_{31} + \overline{\overline{C}}_{36}\overline{d}_{33} + \overline{\overline{C}}_{66}\overline{d}_{36})^{(k)} \mathrm{E}_z^{(k)} \Phi_k dz \end{cases} \tag{15}$$

Upon substitution of Eqs. (14) and (15) into Eq. (13) and back-substitution of the subsequent results into Eq. (6), the governing equations of equilibrium for each region are obtained as follows (the prime sign indicates derivation with respect to x):

$$\begin{cases} \overline{D}_{11}^{kj} U''_j - A_{55}^{kj} U_j + \overline{D}_{16}^{kj} V''_j - A_{45}^{kj} V_j + (\overline{B}_{13}^{kj} - B_{55}^{jk}) W'_j = 0 \\ \overline{D}_{16}^{kj} U''_j - A_{45}^{kj} U_j + \overline{D}_{66}^{kj} V''_j - A_{44}^{kj} V_j + (\overline{B}_{36}^{kj} - B_{45}^{jk}) W'_j = 0 \\ (B_{55}^{kj} - \overline{B}_{13}^{jk}) U'_j + (B_{45}^{kj} - \overline{B}_{36}^{jk}) V'_j + D_{55}^{kj} W''_j - \overline{A}_{33}^{kj} W_j = -N_z^{k^E} \end{cases} \tag{16}$$

Other region(s) have the similar set of fully coupled equations as like as Eq. (16) all of which must be solved simultaneously to find the unknown parameters of the layerwise displacement field.

2.5. Analytical solution

To find analytical solutions to set of governing equations of equilibrium given in Eq. (16) state space variables are defined as follows:

$$(\{X_1(x)\},...,\{X_6(x)\}) = (\{U(x)\},\{U'(x)\},\{V(x)\},\{V'(x)\},\{W(x)\},\{W'(x)\}) \tag{17}$$

where $\{X_i(x)\}_{(N+1)} = [X_{i_1},...,X_{iN+1}]^T$ $(i = 1,\ldots,6)$. Combination of Eqs. (16) and (17) changes the set of $3(N+1)$ second-order differential equations of equilibrium for each region (i.e., Eqs. (16)) into a set of $6(N+1)$ fully coupled first-order differential equations as below:

$$\{X'\}_{6(N+1)\times 1} = [A]_{6(N+1)\times 6(N+1)} \{X\}_{6(N+1)\times 1} + \{F\}_{6(N+1)\times 1} \tag{18}$$

where $\{X\}$ and $\{X'\}$ are the adjunct vectors of $6(N+1)$ state space variables and their derivatives with respect to x and we have:

$$\{F\}_{6(N+1)\times 1} = \left[\left[0\right],\left[0\right],\left[0\right],\left[0\right],\left[0\right],-[D_{55}]^{-1}\left\{N_z^{k^E}\right\}\right]^T \tag{19}$$

in which the electrical stress resultant $N_x^{k^E}$ is defined in Eq. (15), and $[D_{55}]$ and the coefficient matrix A are introduced in Ref. [14]. Three sets of $6(N+1)$ equations like Eqs. (18) corresponding to three regions of J-2 configuration have to be assembled in the matrix form with regards to the boundary and continuity conditions (i.e., Eq. (7)) to build a system of $3 \times 6(N+1)$ coupled equations. Details on the general and particular solutions of this system can be found in Ref. [13]. When the displacement components are completely determined, they can be used to calculate the interfacial peel and shear stress distributions along the joint length or thickness by direct integration of the equilibrium equations of the three-dimensional elasticity theory (as described in Ref. [13]).

For J-1 configuration, the proposed analytical solutions are compared with results of numerical simulations using the commercial finite element software ABAQUS [37]. The FE model is analyzed in plane-stress condition, considering the fact that the joint width is small enough. The interfacial constraint between the layers is considered as prefect bonding. The adhesive layer, as an isotropic homogeneous solid with two material constants, is modeled using a standard 4-node bilinear plane-stress quadrilateral element with reduced integration (CPS4R). The composite substrate with the specified lamination sequence is modeled using the same element type, while the elastic properties are defined by the general type of engineering constants in all directions as listed in Table 1. The piezoelectric patch is modeled as a composite laminate using a standard 4-node bilinear plane-stress piezoelectric quadrilateral element (CPS4E).

Based on an element size study, the mesh network is refined near the interfaces and around the edges and corners using a bias ratio of 5, which results in a gradual decrease of the elemental size by approaching to the corners and edges, in order to decrease the stress singularities as much as possible. The length of elements far away from the edges and corners is less than 0.27 mm, while around the edges and corners it is almost 0.05 mm. Therefore, the whole model contains more than 13,000 elements. The constant electric charge applied to the piezo patch is modeled as an electric potential with uniform distribution.

3. Results and discussion

In this section, numerical results including the interfacial shear and peel stress as well as the von Mises stress distributions at the lower and upper interfaces and the midline of the adhesive layer are presented for J-1 configuration. For this joint, the results obtained by the proposed formulations are compared with results of simulations using the

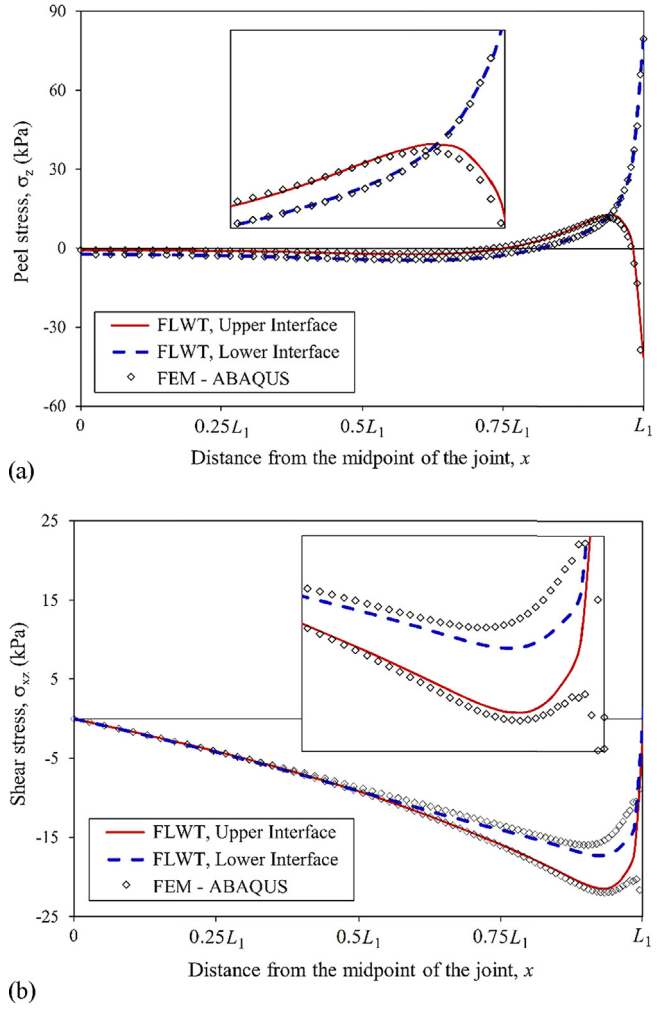

Fig. 3. Interfacial stress distributions along the upper and lower bondlines of J-1 configuration, (a) peel stress σ_z and (b) shear stress σ_{xz}.

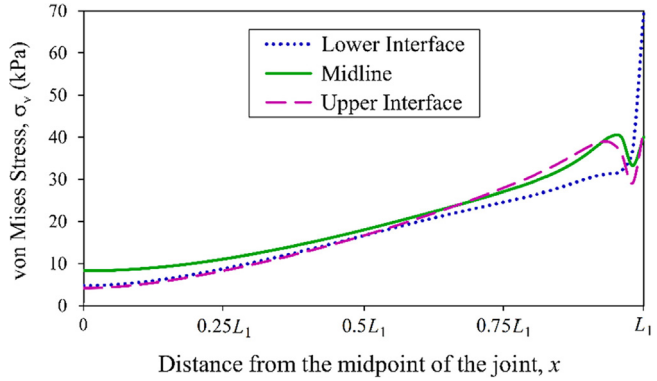

Fig. 4. The von Mises stress distribution along the upper and lower interfaces as well as the midline of the adhesive layer of the J-1 configuration.

commercial finite element software ABAQUS [37]. Moreover, convergence of the results is studied for different numbers of virtual plies. Next, the proposed joint is supposed to contain an interfacial void resulting in J-2 configuration for which the edge effects and convergence speed around the void edges are studied.

Both joints J-1 and J-2 are made up of a piezoelectric patch (PZT-4) bonded to a composite substrate (Graphite-Epoxy) using an adhesive layer (AY103), and are subjected to $E_z = 50$ V/mm. Mechanical and electrical properties of the materials are listed in Table 1. According to

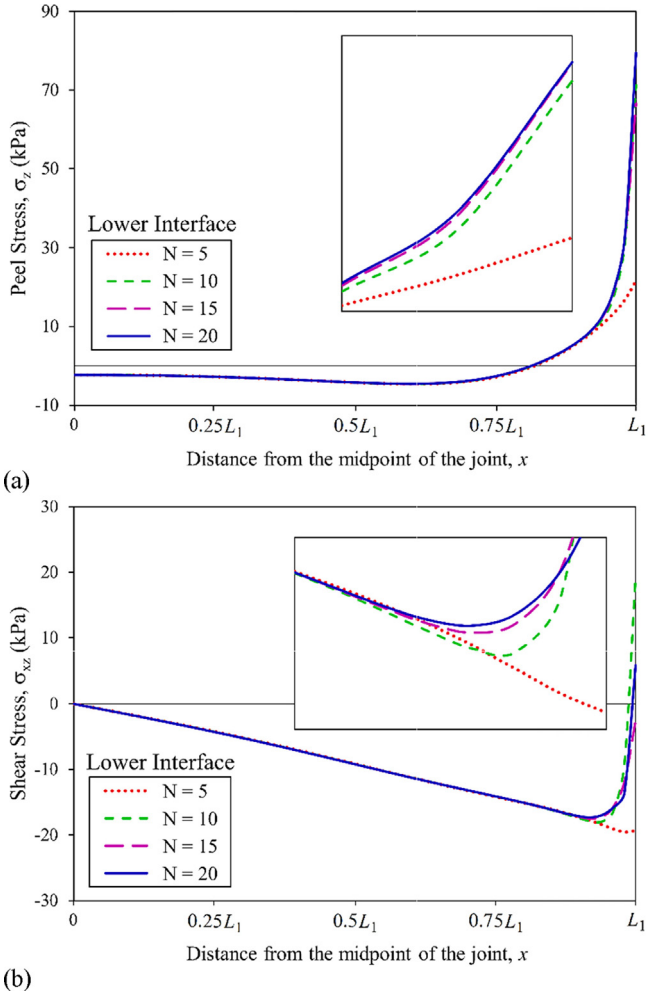

Fig. 5. Convergence of the interfacial stress distributions along the lower bondline of J-1 configuration for different number of virtual plies, N, (a) peel stress σ_z and (b) shear stress σ_{xz}.

Fig. 1 the geometrical details are selected as $t_P = t_A = 1$, $t_S = 3$, $L_1 = 10$, $L_2 = 20$, and $L_V = 0$ and 3 for J-1 and J-2 configurations, respectively (all dimensions in millimeter).

3.1. J-1 configuration

To evaluate the validity of the presented methodology, the distributions of interfacial shear and peel stress distributions along the upper and lower bondlines of the J-1 joint are illustrated in Fig. 3 in comparison with the corresponding results of the finite element simulations.

Fig. 3 shows an excellent agreement between the analytical and numerical peel and shear stress distributions. Fig. 3a obviously illustrates the edge effects in increasing the peel stress value near the end point. Moreover, it shows a rigorous variation of the peel stress from the tensile state at the lower bondline to the compressive state at the upper one in a small zone near the end point due to the edge effects. This variation, however, vanishes sufficiently away from this small zone, where the peel stress decreases to zero. The shear stress obtained by the numerical simulation nevertheless is faced with rigorous variations near the right end point, because of high sensitivity of finite element results to the stress singularities near the edges, corners, and the interfaces of different materials. Whereas, the shear stress obtained by the FLWT decreases truly to zero at the right free end point.

The von Mises stress distribution at the midline of the adhesive layer is demonstrated in Fig. 4. It can be seen in this figure that the maximum

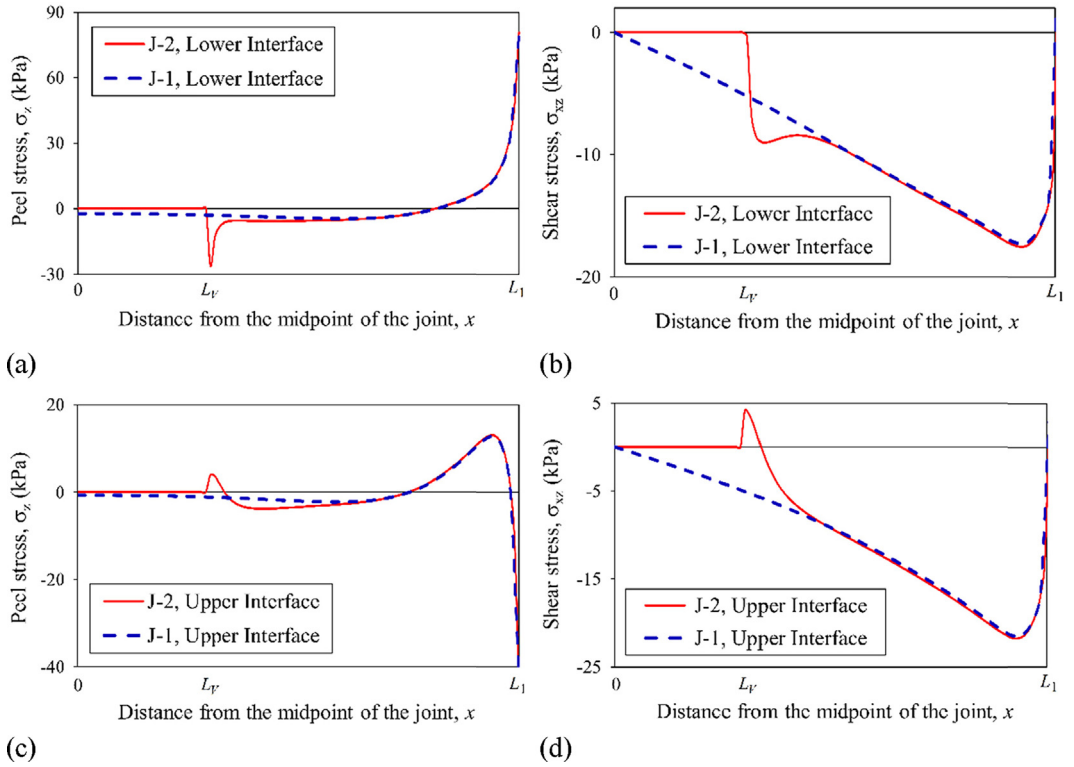

Fig. 6. The interfacial stress distributions on the lower and upper bondlines of the J-1 and J-2 joints, (a, c) peel stress σ_z and (b, d) shear stress σ_{xz}.

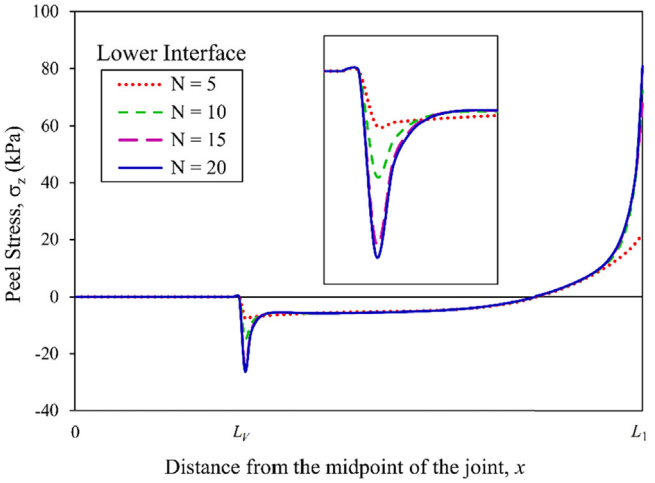

Fig. 7. Convergence of the interfacial peel stress distribution, σ_z, along the lower bondline of J-2 configuration for different number of virtual plies N.

von Mises stress occurs at the endpoint of the bondline, where debonding usually starts.

To study the convergence speed of results, the interfacial peel and shear stress distributions on the lower bondline obtained for different number of virtual plies are demonstrated in Fig. 5. As it is clear, there is no significant difference between the results obtained for $N = 15$ and $N = 20$ (except exactly at the end point caused by stress singularity), and they converges very fast with no need to considerably increase the number of mathematical divisions through the thickness. When $N = 20$, the thickness of mathematical plies equals to $H/N = 250$ μm.

3.2. J-2 configuration

Now suppose a J-2 joint with the same specifications as described for the J-1 joint, except it contains an interfacial void with length of $L_V = 3$ mm. To investigate the edge effects around the void end point (i.e., at $x = L_V$), the interfacial peel and shear stress distributions at the lower and upper bondlines of presumed J-2 joint are illustrated in Fig. 6. For comparison, the corresponding stress distributions of the J-1 joint are also added to the plots. As it can be seen, there is also a considerable increase of the interfacial stresses around the void edge (i.e., at $x = L_V$) caused by the edge effects. Although the peak values at the right end point of the bonding zone (i.e., at $x = L_1$) are still greater than the local peak values around the void edge, it is likely a potential point to start debonding as a result of probable microcracks in this zone.

Fig. 7 depicts the convergence of the peel stress distribution on the lower bondline of the J-2 joint as a convergence study sample for the J-2 configuration. It can be seen that the present method can predict the stresses around the void edge with no need to considerably increase the number of mathematical plies.

To study the effects of void length, L_V, on the interfacial stress distributions and the localized stress concentrations around the void corner as a result of the edge effects, a parametric study on the void length is shown in Fig. 8. Four different joints with J-2 configuration are supposed to contain voids with length of $L_V = 1.5$, 3, 4.5, and 6 mm. The interfacial peel and shear stress distributions at the lower and upper bondlines of the presumed J-2 joints are illustrated in Fig. 8. The peak shear and peel stress values around the void edge increase as the void length increases. Although the edge effects around the void result in local stress concentrations diminishing sufficiently away from its edge, the local peak values around the void, as Fig. 8 shows, may exceed even the global peak stresses of the joint for a particular void length. This clearly indicates the importance of the bonding quality.

4. Conclusions

This paper presented an analytical electromechanical study on the interfacial stress distributions in adhesively bonded composite joints integrated with piezoelectric actuator within the framework of full layerwise theory. A healthy piezo-integrated composite lap joint, J-1, as

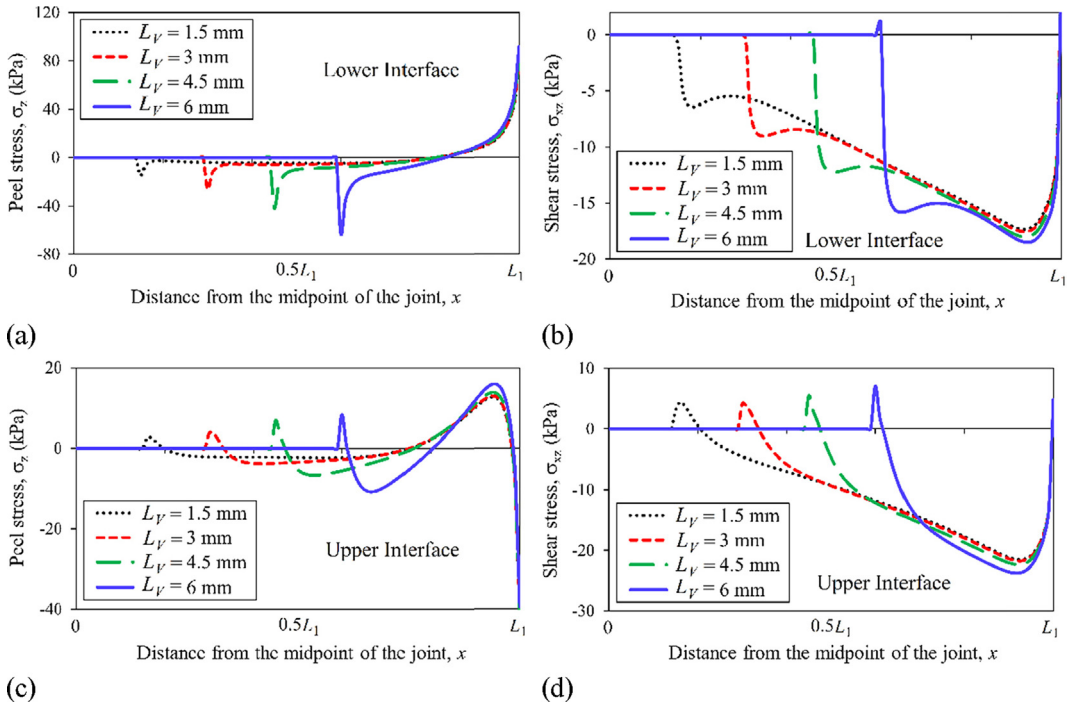

Fig. 8. Effect of different void size on the interfacial stress distributions at the lower and upper bondlines of the J-2 joint, (a, c) peel stress σ_z and (b, d) shear stress σ_{xz}.

well as a defected one containing an interfacial void within the adhesive layer, J-2, were modeled in order to investigate the edge effects near the end-points of the bondline as well as around the void edges. For this purpose, sets of fully coupled governing equations of equilibrium for each joint were derived using the principle of minimum total potential energy and simultaneously solved using the state space approach. Results showed that there is a very good agreement between the results of the proposed method and those of finite element simulations, although the later cannot predict the stresses at the end points, where the bonding is more prone to failure, as accurate as the former because of its high sensitivity to stress singularity near the material and geometrical discontinuities. A good accuracy was also achieved just using a small number of mathematical plies. It was observed that, because of high stress concentrations, the void edges are susceptible places for propagation of probable microcracks and the consequent debonding of piezoelectric patch, which is more challenging when the void length increases.

Acknowledgements

This research did not receive any specific grant from funding agencies in the public, commercial, or not-for-profit sectors.

References

[1] Tichý J, Erhart J, Kittinger E, Přívratská J. Fundamentals of piezoelectric sensorics: mechanical, dielectric, and thermodynamical properties of piezoelectric materials. Germany: Springer, Verlag Berlin Heidelberg; 2010.
[2] Dugnani R, Chang FK. Analytical model of lap-joint adhesive with embedded piezoelectric transducer for weak bond detection. J Intell Mater Syst Struct 2017;28(1):124–40.
[3] Mulligan KR, Quaegebeur N, Masson P, Brault LP, Yang C. Compensation of piezoceramic bonding layer degradation for structural health monitoring. Struct Health Monit 2014;13(1):68–81.
[4] Deligianni A, Hale JM, Kotsikos G. Development of piezoelectric thick-film sensors to be embedded into adhesively bonded joints. Plast Rubber Compos 2016;45(4):173–80.
[5] Gulizzi V, Rizzo P, Milazzo A. On the repeatability of electromechanical impedance for monitoring of bonded joints. AIAA J 2015;53:3479–83.
[6] Malinowski P, Wandowski T, Ostachowicz W. The use of electromechanical impedance conductance signatures for detection of weak adhesive bonds of carbon fibre-reinforced polymer. Struct Health Monit 2015;14(4):332–44.
[7] Zhuang Y, Kopsaftopoulos F, Chang FK. Bondline integrity monitoring of adhesively bonded structures via an electromechanical impedance based approach. Proceedings of the 10th international workshop on structural health monitoring. 2015. CA; USA.
[8] de Medeiros R, Borges EN, Tita V. Experimental analyses of metal-composite bonded joints: damage identification. Appl Adhes Sci 2014;2(1):13.
[9] Ren B, Lissenden CJ. Modal content-based damage indicators for disbonds in adhesively bonded composite structures. Struct Health Monit 2016;15(5):491–504.
[10] Karpenko O, Koricho E, Khomenko A, Dib G, Haq M, Udpa L. Multitechnique monitoring of fatigue damage in adhesively bonded composite lap-joints. AIP Conf Proc 2015;1650(1):1102–11.
[11] Shui G, Wang YS, Huang P, Qu J. Nonlinear ultrasonic evaluation of the fatigue damage of adhesive joints. NDT & E Int 2015;70:9–15.
[12] Flor FR, de Medeiros R, Tita V. Numerical and experimental damage identification in metal-composite bonded joint. J Adhes 2015;91(10–11):863–82.
[13] Yousefsani SA, Tahani M. Relief of edge effects in bi-adhesive composite joints. Compos B Eng 2017;108:153–63.
[14] Yousefsani SA, Tahani M. Analytical solutions for adhesively bonded composite single-lap joints under mechanical loadings using full layerwise theory. Int J Adhes Adhes 2013;43:32–41.
[15] Yousefsani SA, Tahani M. Accurate determination of stress distributions in adhesively bonded homogeneous and heterogeneous double-lap joints. Eur J Mech A Solids 2013;39:197–208.
[16] Selahi E, Tahani M, Yousefsani SA. Analytical solution of stress field in adhesively bonded composite single-lap joints under mechanical loadings. Int J Eng Trans C 2013;27(3):475.
[17] Chadegani A, Batra RC. Analysis of adhesive-bonded single-lap joint with an interfacial crack and a void. Int J Adhes Adhes 2011;31(6):455–65.
[18] Tahani M, Yousefsani SA. On thermomechanical stress analysis of adhesively bonded composite joints in presence of an interfacial void. Compos Struct 2015;130:116–23.
[19] Yang Q, Qin Q, Liu T. Interlayer stress in laminate beam of piezoelectric and elastic materials. Compos Struct 2006;75:587–92.
[20] Zhang J, Zhang B, Fan J. A coupled electromechanical analysis of a piezoelectric layer bonded to an elastic substrate: part I, development of governing equations. Int J Solids Struct 2003;40:6781–97.
[21] Zhang J, Zhang B, Fan J. A coupled electromechanical analysis of a piezoelectric layer bonded to an elastic substrate: part II, numerical solution and applications. Int J Solids Struct 2003;40:6799–812.
[22] Wang SY. A finite element model for the static and dynamic analysis of a piezoelectric bimorph. Int J Solids Struct 2004;41:4075–96.
[23] Maurini C, Pouget J, Dell'Isola F. On a model of layered piezoelectric beams including transverse stress effect. Int J Solids Struct 2004;41:4473–502.
[24] Maurini C, Pouget J, Dell'Isola F. Extension of the Euler-Bernoulli model of piezoelectric laminates to include 3D effects via a mixed approach. Comput Struct 2006;84:1438–58.
[25] Kapuria S. An efficient coupled theory for multilayered beams with embedded piezoelectric sensory and active layers. Int J Solids Struct 2001;38:9179–99.
[26] Luo Q, Tong L. Exact static solutions to piezoelectric smart beams including peel

stresses, I: theoretical formulation. Int J Solids Struct 2002;39:4677–95.
[27] Luo Q, Tong L. Exact static solutions to piezoelectric smart beams including peel stresses, II: numerical results, comparison and discussion. Int J Solids Struct 2002;39:4697–722.
[28] Cheng J, Taheri F. A smart single-lap adhesive joint integrated with partially distributed piezoelectric patches. Int J Solids Struct 2006;43:1079–92.
[29] Cheng J, Wu X, Li G, Taheri F, Pang S. Design and analysis of a smart adhesive single-strap joint system integrated with the piezoelectrics reinforced composite layers. Compos Sci Technol 2007;67:1264–74.
[30] Cheng J, Wu X, Li G, Taheri F, Pang S. Development of a smart composite pipe joint integrated with piezoelectric layers under tensile loading. Int J Solids Struct 2006;43:5370–85.
[31] Cheng J, Wu X, Li G, Pang S, Taheri F. Design and analysis of a smart composite pipe joint system integrated with piezoelectric layers under bending. Int J Solids Struct 2007;44:298–319.
[32] Cheng J, Li G. Stress analyses of a smart composite pipe joint integrated with piezoelectric composite layers under torsion loading. Int J Solids Struct 2008;45:1153–78.
[33] Jin C, Wang X. Analytical modelling of the electromechanical behaviour of surface-bonded piezoelectric actuators including the adhesive layer. Eng Fract Mech 2011;78:2547–62.
[34] Liang W, Rui-xiang B, Cheng Y. Interfacial debonding behavior of composite beam/plates with PZT patch. Compos Struct 2010;92:1410–5.
[35] Reddy JN. Mechanics of laminated composite plates and shells: theory and analysis. 2nd ed. Florida, USA: CRC Press LLC; 2004.
[36] Tahani M. Analysis of laminated composite beams using layerwise displacement theories. Compos Struct 2007;79(4):535–47.
[37] ABAQUS User Manual and Software, Version 6.9-1. Simulia Dassault Systèmes. Providence, RI; 2009.